Design of a Reluctance Synchronous Machine for Saliency Based Position Sensorless Control at Zero Reference Current

W.T. Villet, M.J. Kamper

Department of Electrical and Electronic Engineering
Stellenbosch University
15053830@sun.ac.za, kamper@sun.ac.za

***Abstract*—The saliency dependent position sensorless control capability of reluctance synchronous machine (RSM) drives is investigated in this paper. High frequency injection position sensorless control methods rely on a large enough saliency to track the electrical angle. The RSM has a large saliency within its rated operating regions making it ideal for high frequency injection position sensorless control. It is shown, however, in this paper that the RSM has a limited saliency magnitude at low current, limiting its position sensorless control capability. Design modifications are suggested to increase the saliency of the RSM at zero reference current, thus increasing the drive's position sensorless control capability. These modifications are simulated in a FE package, built and evaluated. The effect of rotor skewing on the position sensorless control capability of the RSM is also evaluated by means of a FE package. A RSM with a skewed rotor is tested to confirm simulation results.**

***Index Terms*—Sensorless control, reluctance synchronous machines, variable speed drives**

NOMENCLATURE AND DEFINITIONS

Symbols:

u, i, ψ	Voltage current and flux linkage
R, L	Resistance and inductance
T_M, Θ	Mechanical torque and inertia
θ_r, ω_r	Rotor- angle and speed
θ_e, ω_e	Electrical- rotor angle and speed
Δ, Σ	Difference and sum

Indices:

s, r	Stator and rotor
a, b, c	Stator phase axes
α, β	Stator fixed cartesian axes
d, q	Rotor fixed direct and quadrature axes
c	Carrier frequency

Scalar values are written in normal letters, e.g. R or τ, vector values are written in small bold letters, e.g. $\mathbf{i}$ or $\boldsymbol{\psi}$, and tensor matrices are written in bold capital letters, e.g. $\mathbf{L}$ or $\mathbf{T}$. Subscripts describe the location of the physical quantity, e.g. R_s is the stator resistance. Superscripts specify the reference frame of the quantity, e.g. $\mathbf{i}_s^{(r)}$ is the stator current vector in the rotor reference frame. Estimated quantities are indicted with a hat, e.g. $\hat{\theta}_e$.

I. INTRODUCTION

Back EMF position sensorless control methods are used with permanent magnet (PM) machines for position estimation at medium to high speeds. With these methods, however it is impossible to estimate the electrical angle at standstill and low speeds due to a lack of back EMF [1]. High frequency injection position sensorless control methods can be used at standstill and low speeds to estimate the electrical angle.

High frequency injection position sensorless control methods are used to estimate the electrical angle of salient pole machines. Literature, however, shows that certain design aspects of PM machines can negatively affect the inductance saliency which is necessary to perform saliency based position sensorless control [2] [3].

The effect of the identified design limitations with regard to inductance saliency, are investigated for reluctance synchronous machines (RSMs). Finite element (FE) software is used to compare three RSM drives with three different rotor structures and evaluate their position sensorless control capability. One of the evaluated RSM drives is measured and compared to simulation results. The results of this RSM drive are used as a basis for comparison. The aim is to improve the position sensorless control capability of the RSM drive at zero reference current by modifying the rotor structure. Finally, the effect of a full slot pitch skew on the position sensorless control capability of the drive is investigated.

II. ALTERNATING HIGH FREQUENCY INJECTION METHOD

This position sensorless control method makes use of an amplitude modulation scheme to track the electrical angle of the RSM by superimposing a high frequency voltage vector onto the fundamental control voltage vector in the estimated rotary reference frame [4]. With proper demodulation it is possible to track the anisotropy position which rotates at the same angular frequency as the rotor [5].

978-1-4673-4569-9/13/$31.00

The only source of flux of the RSM is the stator coils. Hence the RSM is described electrically by the stator voltage equation of (1). Under high frequency excitation the RSM stator voltage equation consist of only an inductance term as in (2) [4] [6].

$$\mathbf{u}_s^{(s)} = R_s \mathbf{i}_s^{(s)} + \dot{\boldsymbol{\psi}}_s^{(s)} \tag{1}$$

$$\mathbf{u}_{sc}^{(r)} = \mathbf{L}^{(r)} \frac{d\mathbf{i}_{sc}^{(r)}}{dt} \tag{2}$$

$\mathbf{L}^{(r)}$ is the tangential inductance matrix [6]. The injected carrier voltage vector is as defined in (3) when implementing alternating HF injection position sensorless control,. The stator current is used as feedback, thus the measured current in the estimated rotary reference frame (as dissipated by superscript $\hat{r}$) is as shown in (4) [6] [7].

$$\mathbf{u}_{sc}^{(\hat{r})} = \begin{bmatrix} u_c cos(\omega_c t) \\ 0 \end{bmatrix} \tag{3}$$

$$\begin{aligned} \mathbf{i}_{sc}^{(\hat{r})} &= \mathbf{L}^{(\hat{r})^{-1}} \int \mathbf{u}_{sc}^{(\hat{r})} dt \\ &= \frac{u_c sin(\omega_c t)}{L_d L_q \omega_c} \left(L_\Sigma \begin{bmatrix} 1 \\ 0 \end{bmatrix} - \Delta L \begin{bmatrix} cos(2\Delta\theta_e) \\ sin(2\Delta\theta_e) \end{bmatrix} \right) \end{aligned} \tag{4}$$

where

$$L_\Sigma = \frac{(L_d + L_q)}{2} \qquad and \qquad \Delta L = \frac{(L_d - L_q)}{2} \tag{5}$$

L_Σ is the mean inductance and ΔL the inductance saliency (difference inductance). $\Delta\theta_e = \theta_e - \hat{\theta}_e$ is the electrical position estimation error. If it is assumed that the position estimation error is small enough it can be assumed that $sin(\Delta\theta_e) \approx \Delta\theta_e$ and $cos(\Delta\theta_e) \approx 1$. These simplifications coupled with proper demodulation leads to (6).

$$\mathbf{i}_{s(demod)}^{(\hat{r})} = \frac{u_c}{2L_d L_q \omega_c} \left(L_\Sigma \begin{bmatrix} 1 \\ 0 \end{bmatrix} - \Delta L \begin{bmatrix} 1 \\ 2\Delta\theta_e \end{bmatrix} \right) \tag{6}$$

Now (6) shows that the q-axis current has information regarding the position estimation error. The q-axis current can be used to drive a phase locked loop (PLL) to track the electrical rotor angle [5] [6]. Equation (6) shows that the electrical position estimation error is scaled by the magnitude of the inductance saliency. This implies that it will be impossible to track the electrical angle if $L_d = L_q$.

III. Degradation of position sensorless control performance

According to [2] and [8] there are two effects that can distort the position sensorless control capability of PM drives, namely, saturation and cross-coupling effects. The magnitude of the inductance saliency, ΔL, decreases as the flux saturates within the machine until position sensorless control is not possible any more. This saturation effect occurs when the machine is loaded.

It is found that cross-coupling between the d- and q-axes is caused by the asymmetrical saturation of the rotor [3]. To investigate the distortion caused by the cross coupling effect in RSMs, FE analysis is done on three rotor structures as shown in Figure 1. To adhere to convention as chosen by [2], these three rotors structures are referred to as the ideal-, Figure 1(a), lateral rib-, Figure 1(b), and central rib rotors, Figure 1(c). The flux density maps of Figures 1(a) and 1(b) at rated conditions are similar and symmetrical, as also identified by [2]. However, high distortion is present in Figure 1(c) where the flux lines concentrate in the central rib, causing asymterical saturation and thus increasing the cross coupling between the d- and q-axes. If the concentration on the central rib is high enough it can cause the position sensorless control method to misalign with the d-axis of the rotor. This phenomena is referred to as saliency shift in [9] and [10].

IV. Evaluation of the RSM rotor structure with regard to inductance saliency

The investigated RSM has a 2-pole pair rotor with a 3-phase distributed winding standard induction machine stator. This 1.2 kW RSM is designed and built at the University of Stellenbosch. The RSM geometry is that of the unskewed lateral rib configuration as seen in Figure 1(b).

The RSM is a salient pole machine ($L_d \neq L_d$) making it ideal for saliency dependent position sensorless control methods like the alternating high frequency injection method. To prove this, a FE and measured analysis are made of this RSM to investigate its position sensorless capability. The uncoupled d- and q-axis flux linkages are used to aid this investigation. The d- and q-axis tangential inductances are calculated as:

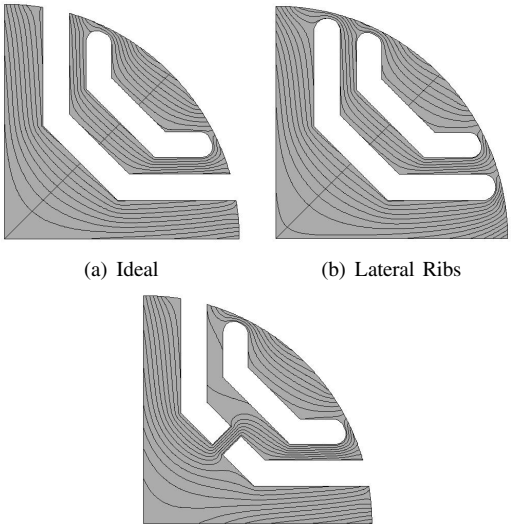

(a) Ideal (b) Lateral Ribs

(c) Central Ribs

Fig. 1. Cross coupling effect on (a) the ideal- , (b) lateral rib- and (c) cental rib rotor configurations.

$$L_d = \frac{\Delta\psi_d}{\Delta i_d}; \psi_d(i_d, 0) \tag{7}$$

$$L_q = \frac{\Delta\psi_q}{\Delta i_q}; \psi_q(0, i_q) \tag{8}$$

Both the d- and q-axis flux linkages are functions of both i_d and i_q [2]. With the described method of inductance calculation it is possible to investigate the saliency of the RSM with regard to the geometry of the design, minimising the cross coupling effects. The results of the simulated and measured analysis of this rotor structure are shown in Figure 2. The first frame shows the uncoupled flux linkages as a function of current and the second frame the tangential inductances. It is clear that there are some irregularities between the measured and the simulated results. This might be due to an uncertainty regarding the rotor- and stator steel. Also contributing to the irregularities is the fact that the inductances are calculated as partial derivatives. This implies that slight gradient deviation of the flux linkage causes large deviation of the inductance. The important aspect regarding these results is that the shape of the flux linkages of the measured and simulated results are satisfactorily similar.

The measured and simulated inductance saliency (ΔL) are shown in the second frame. These results show that the magnitude of the saliency is not large enough for position sensorless control when the machine is loaded . This is due to saturation of the flux in the machine as described in the previous section. The gradients of the flux linkages approach a horizontal gradient as a result of saturation causing the saliency to decrease. A second problem area is at zero current where $L_d \approx L_q$. This is due to $\psi_d(i_d, 0)$ and $\psi_q(0, i_q)$ having the same gradient.

The effects of these two problem areas play a large role in the performance of the position sensorless controlled drive. The maximum torque of the position sensorless controlled drive is limited due to the saturation under load conditions. The limited saliency at zero current prevents the position sensorless control method from tracking the electrical angle. A suitable example of where this could be problematic is when speed or torque steps are applied externally to the sensorless controlled RSM drive at standstill. The HF injection method is unable to track the electrical angle, and thus loses control of the machine. To counter this limitation the current vector can be chosen in such a way that there is always a q-axis current to saturate the q-axis flux. It is found that the minimum q-axis current necessary is 0.2 $[p.u]$. Although effective, this method is not energy efficient due to the current vector not always following the maximum torque per ampere locus. This method of course also implies that there is always current in the machine even at standstill or at no load.

Applications like electric vehicles that operate regularly at standstill conditions would benefit from a RSM design that does not rely on q-axis flux saturation for position sensorless control. The urban dynamometer driving schedule (UDDS) is a dynamometer test on fuel economy in urban driving conditions. The cycle simulates an urban route of 12.07 km in Fig. 3. This graph clearly shows that there are various instances where a vehicle comes to standstill in this route [11]. Electric drives for electric vehicles are thus one example of an application that can benefit from a RSM design with a high inductance saliency magnitude at zero current.

V. RSM DESIGN FOR HIGH SALIENCY AT ZERO REFERENCE CURRENT

The identified problems of saturation and saliency shift caused by cross-coupling exist for PM machines and RSMs. These problems are already addressed for PM machines with proposed solutions for preventing saturation and increasing the saliency [2], [3], [8]–[10], [12], [13]. In the previous section it was explained that the magnitude of the RSM's saliency at zero current is not sufficient, limiting its position sensorless control ability. The limited saliency of the RSM at zero current is investigated in this work so as to to increase the energy efficiency of the position sensorless controlled drive. The stator of the investigated RSM is a standard induction machine stator, thus the focus is on rotor modifications that can improve on the magnitude of the saliency at zero reference current.

The central rib rotor configuration is investigated as an alternative to the lateral rib configuration for high saliency at zero current. Although it was proven in the previous section

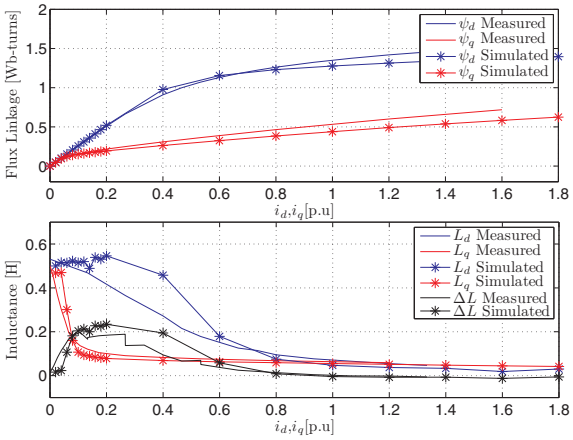

Fig. 2. Measured flux linkages and inductances vs simulated results of the lateral rib rotor configuration.

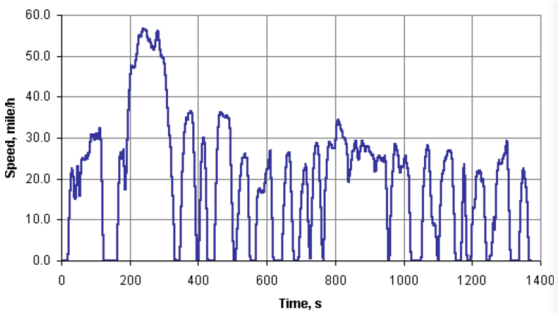

Fig. 3. Urban dynamometer driving schedule (UDDS) for 12.07 km [11].

that this configuration causes problems for the sensorless methods when the machine is loaded, it is still unsure of this structure's saliency characteristics at zero current. This structure is also simulated as unskewed to compare to the lateral rib configuration. The uncoupled flux linkages and inductances as a function of current are shown in Fig. 4. The simulation results show that the central rib configuration also suffers from a lack of saliency at no load.

The second investigated configuration is that of the ideal rotor structure. Again this configuration is simulated with the rotor configuration unskewed. The FE results of the uncoupled flux linkages and inductances of the ideal rotor are compared with the simulation results of the lateral rib configuration in Fig. 5. This graph shows that $\psi_d(i_d, 0)$ and $\psi_q(0, i_q)$ have different gradients at low current, resulting in a high saliency due to $L_d \neq L_q$. Not only does this configuration have a large saliency magnitude at zero current, it also has a more constant saliency magnitude over current than the lateral rib configuration. These results suggest that the geometry of the ideal rotor configuration has, as expected, a higher saliency at zero current than that of the other two configurations.

VI. Skewing of the Rotor

In [12] the effect of skewing of a PM machine is investigated. The skew in [12] is a quarter of a slot pitch and the findings were that skewing has little or no effect on the position sensorless control capability of the machine. It is important to investigate the position sensorless control capability of the RSM with the rotor skewed one stator slot pitch. Both the lateral rib- and ideal rotor configuration are simulated in five sub-machines to simulate a full slot pitch skewed rotor. The saliency acquired from the simulation results are shown in Fig. 6. These results show that there is very little deviation of the saliency when a RSM rotor is skewed one stator slot pitch and that it possesses all the necessary characteristic for successful position sensorless control.

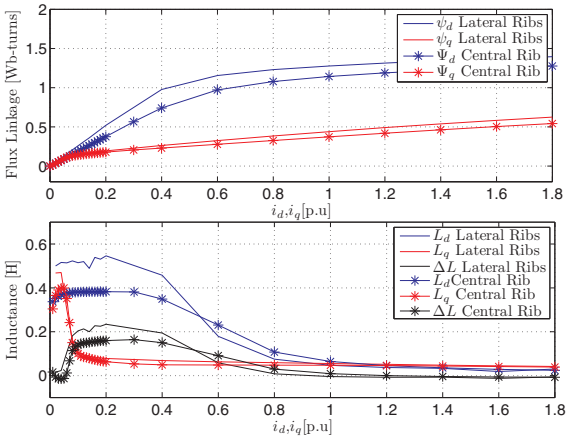

Fig. 4. Simulated flux linkages and inductances of the lateral rib configuration vs. the central rib configuration.

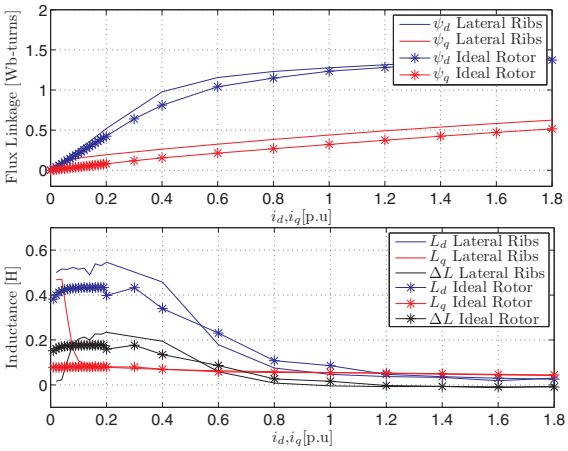

Fig. 5. Simulated flux linkages and inductances of the lateral rib configuration vs. the ideal rotor configuration.

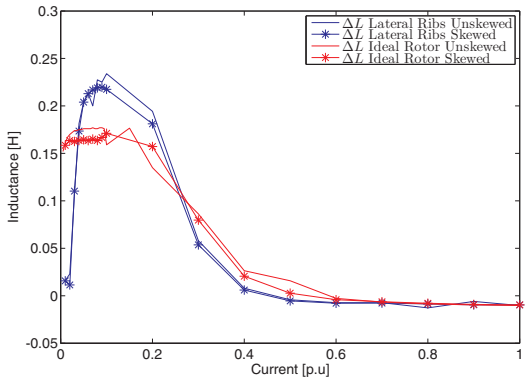

Fig. 6. Simulated saliency comparison of the skewed and unskewed lateral rib- and ideal rotor configurations.

VII. Ideal Rotor Configuration

A. Construction of the ideal rotor configuration

Simulation results suggest that the ideal rotor configuration will perform well under position sensorless control with zero reference current. It is decided to build the unskewed and skewed ideal rotors and evaluate the position sensorless control capability of these drives. The obvious problem is that a piece of the rotor steel "floats" in the air. To overcome this problem a novel solution is implemented. Slots that match the flux barriers of the rotor laminations are cut into one of the end-caps of the rotor. With this it is possible to fill the axial length of the rotor with an epoxy-resin. Epoxy-resin is very strong, but is not recognised as an adhesive substance, thus it will not be able to hold the floating piece of iron in place. To take advantage of the strength of epoxy-resin, small cut outs and iron snags are laser cut into the laminations as shown on the CAD design in Fig. 7. These cutouts help the epoxy to grip the floating piece of iron and prevent it from moving away. After allowing the epoxy to harden a lathe is used to cut out the ribs. The unskewed rotor without its lateral ribs is shown in Figure 8.

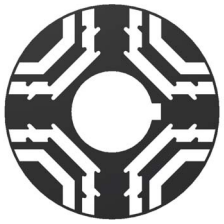

Fig. 7. CAD sketch of proposed RSM rotor lamination.

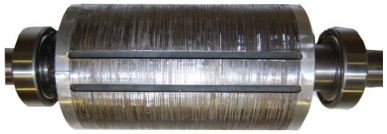

Fig. 8. Epoxy filled RSM rotor without lateral ribs.

B. Measured evaluation of the unskewed ideal rib configuration

Figure 9 shows the simulated and the measured uncoupled flux linkages and inductances of the unskewed ideal rib configuration RSM. The measured results correlate well with the simulated results. More importantly these results show that this configuration has a high saliency at zero reference current. To confirm this a simple test is devised to test the drive's position sensorless control capability. The alternating HF injection method is implemented on this drive with a reference current of zero ampere, while an induction machine (IM) is used to drive the RSM at a constant speed. It is not possible to control the lateral rib rotor RSM sensorless under these conditions due to the small magnitude of the saliency. With the unskewed ideal rib configuration, the high frequency injection method tracks the electrical angle effectively as shown in Figure 10. A small q-axis current exists as a result of the HF voltage excitation, allowing the demodulation scheme to track the electrical angle. No additional q-axis current is thus required to saturate the q-axis flux at standstill and low speeds.

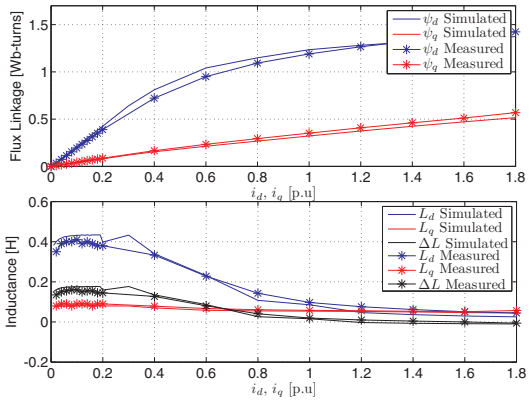

Fig. 9. Simulated results vs. measured results of the unskewed ideal rib configuration.

C. Measured evaluation of the skewed ideal rib configuration

The measured and simulated uncoupled flux linkages and inductances of the skewed RSM are shown in Fig. 11. Again the measured results correlate well with the simulated results. These results show that this configuration has a large enough saliency to perform positions sensorless control at low reference currents. This is confirmed by the same HF injection test performed on the the unskewed rotor. The results of this test in Fig. 12 clearly show that even though the rotor is skewed one slot pitch, position sensorless control is still possible and that there exists a high enough saliency under no load conditions to estimate the electrical angle.

D. Concluding thoughts on the ideal rotor RSM design

No measures were taken to protect a "fragile" rotor design during the testing procedures of the two constructed rotors. These two designs underwent harsh testing procedures, most of them at above rated conditions. No damages was caused to

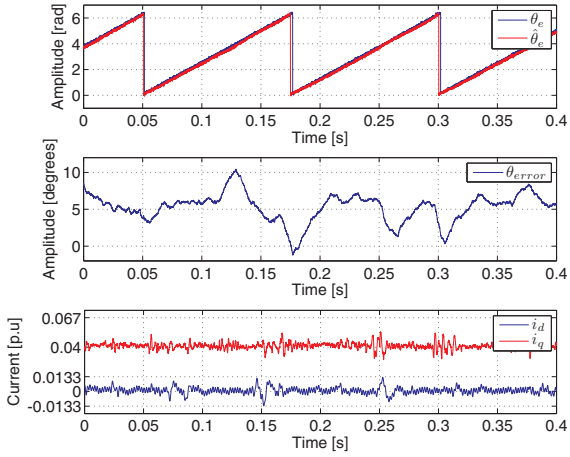

Fig. 10. Measured results of the HF injection method implemented on the unskewed ideal configuration RSM design. Reference current of 0 A while driven by the IM drive at constant speed.

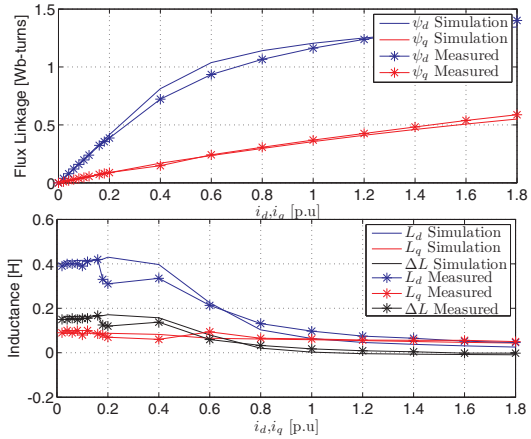

Fig. 11. Simulated results vs. measured results of the skewed ideal rib configuration.

the rotor as a result of these tests. It seems that the epoxy-hook combination ensures stability of the rotor.

Figure 13 compares the measured saliency of the three measured RSM designs. This graph clearly shows that the two ideal rotor configurations have an increased saliency under no load conditions as well as a higher saliency under loaded conditions.

VIII. Conclusion

Two design aspects that distort the high frequency injection position sensorless control capability of RSM drives are discussed, namely saturation and saliency shift. It is shown that these two phenomena are not exclusive to permanent magnet machines, but affect RSM drives as well. A third problem area was identified when investigating the position sensorless control capability of a custom built RSM with a lateral rib configuration. This problem area occurs at zero reference current where the magnitude of the saliency is too small for position sensorless control.

A FE package is used to investigate alternative unskewed rotor structures with a high saliency at no load. FE results indicated that the ideal rotor configuration has a large enough saliency at no load for position sensorless control. This rotor configuration was constructed with a novel epoxy-resin rotor. Measured results correlated well with the simulation results and showed that the new proposed design has a higher saliency at zero reference current. A simple HF injection position sensorless control testing procedure proved that no additional q-axis current is necessary to saturate the q-axis flux under no load conditions.

The position sensorless control ability of the lateral rib and ideal rotor configurations is also investigated with a rotor that is skewed by one stator slot pitch. Simulation and measured results confirmed that the RSM drive with the skewed ideal rotor configuration possess the necessary characteristics for position sensorless control. These results also showed that the ideal rotor configuration retains its large saliency at zero reference current when skewed.

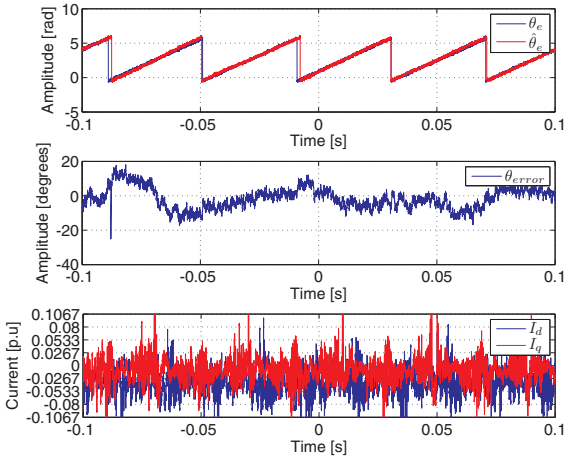

Fig. 12. Measured results of the HF injection method implemented on the skewed ideal configuration RSM design. Reference current of 0 A while driven by the IM drive at constant speed.

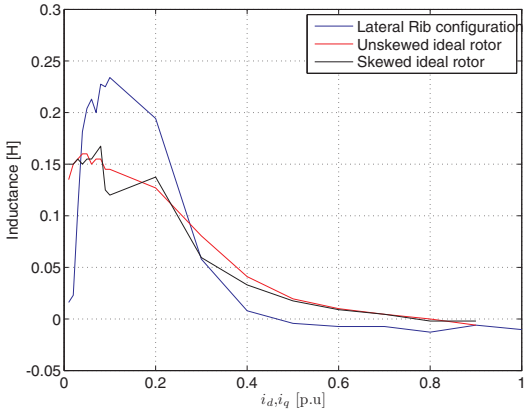

Fig. 13. Measured saliency of the three RSM designs.

References

[1] F. Genduso, R. Miceli, C. Rando, and G. Galluzzo, "Back emf sensorless-control algorithm for high-dynamic performance pmsm," *Industrial Electronics, IEEE Transactions on*, vol. 57, no. 6, pp. 2092 –2100, june 2010.

[2] N. Bianchi and S. Bolognani, "Influence of rotor geometry of an interior pm motor on sensorless control feasibility," in *Industry Applications Conference, 2005. Fourtieth IAS Annual Meeting. Conference Record of the 2005*, vol. 4, oct. 2005, pp. 2553 – 2560 Vol. 4.

[3] N. Bianchi, S. Bolognani, and M. Zigliotto, "Design hints of an ipm synchronous motor for an effective position sensorless control," in *Power Electronics Specialists Conference, 2005. PESC '05. IEEE 36th*, june 2005, pp. 1560 –1566.

[4] D. Raca, P. Garcia, D. Reigosa, F. Briz, and R. Lorenz, "A comparative analysis of pulsating vs. rotating vector carrier signal injection-based sensorless control," in *Applied Power Electronics Conference and Exposition, 2008. APEC 2008. Twenty-Third Annual IEEE*, feb. 2008, pp. 879 –885.

[5] M. Linke, R. Kennel, and J. Holtz, "Sensorless speed and position control of synchronous machines using alternating carrier injection," in *Electric Machines and Drives Conference, 2003. IEMDC'03. IEEE International*, vol. 2, June 2003, pp. 1211 – 1217 vol.2.

[6] W. Hammel and R. Kennel, "Position sensorless control of PMSM by synchronous injection and demodulation of alternating carrier voltage," in *Sensorless Control for Electrical Drives (SLED), 2010 First Symposium on*, july 2010, pp. 56 –63.

[7] R. Leidhold and P. Mutschler, "Improved method for higher dynamics in sensorless position detection," in *Industrial Electronics, 2008. IECON 2008. 34th Annual Conference of IEEE*, nov. 2008, pp. 1240 –1245.

[8] N. Bianchi, S. Bolognani, J.-H. Jang, and S.-K. Sul, "Comparison of pm motor structures and sensorless control techniques for zero-speed rotor position detection," *Power Electronics, IEEE Transactions on*, vol. 22, no. 6, pp. 2466 –2475, nov. 2007.

[9] J. Arellano-Padilla, C. Gerada, G. Asher, and M. Sumner, "Inductance characteristics of pmsms and their impact on saliency-based sensorless control," in *Power Electronics and Motion Control Conference (EPE/PEMC), 2010 14th International*, sept. 2010, pp. S1–1 –S1–9.

[10] C. Gerada, J. Padilla, M. Sumner, and T. Raminosoa, "Loading effects on saliency based sensorless control of pmsms," in *Electrical Machines and Systems, 2009. ICEMS 2009. International Conference on*, nov. 2009, pp. 1 –6.

[11] DiesleNet, "Emission Test Cycles," http://www.dieselnet.com/standards/cycles/ftp72.php.

[12] N. Bianchi and S. Bolognani, "Sensorless-oriented-design of pm motors," in *Industry Applications Conference, 2007. 42nd IAS Annual Meeting. Conference Record of the 2007 IEEE*, sept. 2007, pp. 668 –675.

[13] J. Bottomley, C. Gerada, and M. Sumner, "Electrical machine design for optimal self-sensing properties of spmsms," in *Power Electronics, Machines and Drives (PEMD 2012), 6th IET International Conference on*, march 2012, pp. 1 –5.